Water partitioning in the Earth's mantle

Toru Inoue[1], Tomoyuki Wada[1], Rumi Sasaki[1], Hisayoshi Yurimoto[2]

[1]Geodynamics Research Center, Ehime University, Bunkyo-cho 2-5,
Matsuyama, Ehime 790-8577, Japan
[2]Division of Earth and Planetary Sciences, Hokkaido University,
Sapporo 060-0810, Japan

Physics of the Earth and Planetary Interiors 183 (2010) 245-251

Abstract We have conducted H_2O partitioning experiments between wadsleyite and ringwoodite and between ringwoodite and perovskite at 1673K and 1873K, respectively. These experiments were performed in order to constrain the relative distribution of H_2O in the upper mantle, the mantle transition zone, and the lower mantle. We successfully synthesized coexisting mineral assemblages of wadsleyite-ringwoodite and ringwoodite-perovskite that were large enough to measure the H_2O contents by secondary ion mass spectrometry (SIMS). Combining our previous H_2O partitioning data (Chen et al., 2002) with the present results, the determined water partitioning between olivine, wadsleyite, ringwoodite, and perovskite under H_2O-rich fluid saturated conditions are 6: 30: 15 : 1, respectively. Because the maximum H_2O storage capacity in wadsleyite is ~3.3 wt% (e.g. Inoue et al, 1995), the possible maximum H_2O storage capacity in the olivine high pressure polymorphs are as follows: ~0.7 wt% in olivine (upper mantle just above 410 km depth), ~3.3 wt% in wadsleyite (410-520 km depth), ~1.7 wt% in ringwoodite (520-660 km depth), and ~0.1 wt% in perovskite (lower mantle). If we assume ~0.2 wt% of the H_2O content in wadsleyite in the mantle transition zone estimated by recent electrical conductivity measurements (e.g. Dai and Karato, 2009), the estimated H_2O contents throughout the mantle are as follows; ~0.04 wt% in olivine (upper mantle just above 410 km depth), ~0.2 wt% in wadsleyite (410-520 km depth), ~0.1 wt% in ringwoodite (520-660 km depth) and ~0.007 wt% in perovskite (lower mantle). Thus, the mantle transition zone should contain a large water reservoir in the Earth's mantle compared to the upper mantle and the lower mantle.

Key words: mantle, olivine, wadsleyite, ringwoodite, perovskite, hydrous wadsleyite, hydrous ringwoodite, high pressure phase transformation, partitioning of H_2O

1. Introduction

Water, the most abundant volatile component on the Earth's surface, has been supplied to the Earth's mantle by subducting slabs from the lithosphere (e.g. Irifune et al.,1998; Ohtani et al., 2004). Because water influences the physical properties and melting temperature of minerals, it is important to constrain the potential amount of water in nominally anhydrous phases at various depths in the Earth's mantle.

Olivine (α-phase) and the high pressure polymorphs of olivine are the most abundant minerals in the upper mantle, and the high-pressure polymorphs of olivine, wadsleyite (β-phase), and ringwoodite (γ-phase), can contain up to 2-3 wt% of H_2O in their crystal structures (e.g. Inoue et al., 1995, 1998; Kohlstedt et al., 1996). However, the partitioning data of H_2O between these minerals are few except for the olivine-wadsleyite transformation (Chen et al., 2002) and ringwoodite-perovskite transformation (Bolfan-Casanova et al., 2003). We have determined the partitioning of H_2O between wadsleyite and ringwoodite and between ringwoodite and perovskite at 1673K and 1873K, respectively. These temperatures are close to typical mantle temperature proposed by Brown and Shankland (1981) and Katsura et al. (2009) at the 520 km and 660 km seismic discontinuity. We have also ascertained the relative distribution of H_2O among the upper mantle, the mantle transition zone, and the lower mantle.

2. Experimental

High-pressure experiments were conducted in an MA-8 type (Kawai-type) high-pressure apparatus at Ehime University. The truncation edge lengths (TEL) of the cubic anvils were 3.5 and 2.5 mm for the experiments on wadsleyite-ringwoodite and ringwoodite-perovskite, respectively. We used semi-sintered magnesia that was doped with 17 wt % CoO and $LaCrO_3$ as the pressure medium, and ZrO_2 was used as the thermal insulator. We adopted a cylindrical platinum (Pt) or rhenium (Re) heater with a wall thickness of ~30 μm. The typical cell assembly used with TEL of 3.5 mm is shown in Fig. 1.

The starting materials were a mixture of $Mg(OH)_2$, Fe_2SiO_4 and SiO_2 reagent with the

chemical composition of $(Mg_{0.8}Fe_{0.2})_2SiO_4$ plus 15.8 wt% H_2O (Table 1). Thus, H_2O was introduced by $Mg(OH)_2$, and ferrous iron was introduced by Fe_2SiO_4 because wustite ($Fe_{1-X}O$) is non-stoichiometric. The reason we selected such large water content was to enhance the crystal growth and to make it possible to measure the H_2O content precisely by secondary ion mass spectroscopy (SIMS). In addition, the reason we selected the olivine composition of $(Mg_{0.8}Fe_{0.2})_2SiO_4$ was to enhance the coexisting region of wadsleyite-ringwoodite and ringwoodite-perovskite in order to obtain the sample.

A corresponding anhydrous starting material was also prepared. The appropriate mechanical mixture of Mg_2SiO_4 and Fe_2SiO_4 powders was used for the composition of $(Mg_{0.8}Fe_{0.2})_2SiO_4$. Both anhydrous and hydrous samples were enclosed in a welded $Au_{75\%}Pd_{25\%}$ alloy capsule separately before loading into a high pressure cell in order to avoid the loss of both water and iron. Platinum is often used as capsule material, but it absorbs iron significantly. Therefore, we used Au75%Pd25% to make the loss of Fe less, which is superior to Pt in an iron bearing system, as the capsule material.

Temperature was measured with a $W_{97}Re_3$-$W_{75}Re_{25}$ thermocouple junction placed in the center of the furnace assembly. The fluctuation of temperature throughout the run was kept within ±5 ℃ in each condition, but no pressure correction was made for the emf of the thermocouple.

Careful pressure calibration was done on the basis of the present anhydrous experiments of the wadsleyite-ringwoodite phase transition based on the thermochemical phase diagram (Akaogi et al., 1989) at 1673K, and the postspinel phase transition (Ito and Takahashi, 1989) at 1873K. Therefore, the pressure conditions for the coexisting run products wadsleyite-ringwoodite and ringwoodite-perovskite were determined by fitting our anhydrous compositional data on the loop by Akaogi et al.(1989) and Ito and Takahashi (1989). In this case, the relative pressure precision in the runs with the coexisting wadsleyite-ringwoodite and coexisting ringwoodite-perovskite under anhydrous conditions is estimated to be about 0.05 GPa, and about 0.2 GPa in runs without co-existing phases.

In high-pressure and high-temperature experiments, pressure was applied first to the target ram loads, then the temperature was kept constant for 20-120 minutes before quenching by turning off power to the furnace, and then the run was quenched by

99 turning off the electric power. The recovered charges were polished for phase
100 identification and chemical analysis.
101 The phases were identified by a micro-focused X-ray diffractometer and by
102 micro-Raman spectroscopy. The chemical compositions were determined by EPMA and
103 the water content of the minerals was measured by SIMS at Hokkaido University.
104 The SIMS instrument used in the present study was the Cameca IMS-3F ion mass
105 microanalyzer. The polished samples were coated with a gold film 300 Å in thickness
106 for SIMS analysis. A primary beam operated at ~10 nA, 12.5 kV $^{16}O^-$ was focused to
107 form an ~30 μm spot on the sample, and the secondary $^1H^+$ and $^{30}Si^+$ ions were
108 collected from the center region (10 μm in diameter) of the sputtered area using a
109 mechanical aperture to minimize artifacts arising from hydrogen adsorption on the
110 polished sample surface. The H_2O content of samples was calibrated from relative
111 intensities of $^1H^+/^{30}Si^+$ using an empirical linear relationship (Yurimoto et al., 1989). We
112 used natural amphibole crystal with a water content of 1.66 wt % for a standard, which
113 was determined by a hydrogen gas manometry method with the accuracy of ±0.1 wt%
114 (Miyagi and Yurimoto, 1995). In addition, San Carlos olivine was used for the
115 background H intensities, because the H concentration is considerably small (10-60
116 ppm: Kurosawa et al. 1997), compared with the present H concentration in our samples.
117 We obtained a depth profile of the intensity of $^1H^+$ and $^{30}Si^+$ with time. The
118 steady-state hydrogen emission achieved depends on the H concentration, but usually it
119 is achieved after 30-60 minute bombardments of the primary ions with H_2O
120 concentration of ~1 wt%. The uncertainty of the H_2O content in the present analysis is ~
121 ±10%, which mainly comes from the scattering of the measured $^1H^+/^{30}Si^+$ value for
122 several standard measurements, probably because of the slightly chemical heterogeneity
123 of the present natural amphibole standard. More details for the SIMS measurement are
124 described in Miyagi and Yurimoto (1995), and the water content and the chemical
125 composition of the present amphibole standard was shown in Table 1 (ICH) of Miyagi
126 et al. (1998).
127
128 **3. Results and discussion**
129 The experimental conditions and results are summarized in Tables 2 and 3. The
130 experiments were conducted at conditions of 14.6-17.0 GPa and 1673K for the
131 wadsleyite-ringwoodite experiment and ~23 GPa and 1873K for the

ringwoodite-perovskite experiments. The heating durations were 20-120 minutes.

All experiments were performed under H_2O-rich fluid (melt) saturated conditions where solid phases coexisted with a hydrous melt, as evidenced by fibrous crystals and spinifex texture in the quench product. These results show the formation of liquid under all conditions.

Note that at the present experimental conditions in the silicate-H_2O system, H_2O-bearing silicate melt (liquid) and H_2O-rich aqueous fluid cannot be distinguished from each other because of the existence of the second critical end point (e.g. Mibe et al., 2007). So the terminology of melt (liquid) and fluid in this paper has the same meaning.

3-1. The effect of water on the phase boundary between wadsleyite and ringwoodite

We observed the coexistence of wadsleyite and ringwoodite at pressures of 15.6 to 16.5 GPa under anhydrous conditions, whereas the coexistence of both wadsleyite and ringwoodite were not observed below 16.4 GPa under hydrous conditions (Table 2). This shows that the phase boundary between wadsleyite and ringwoodite moves to higher pressure under water-bearing conditions.

Table 4 shows the Fe/(Mg+Fe) in wadsleyite and ringwoodite and the corresponding partition coefficient at each pressure. We define the partition coefficient, Kd, as $(Fe/Mg)_{\gamma}/(Fe/Mg)_{\beta}$. The Kds were ~1.6-1.7 in both the anhydrous and hydrous systems, which are consistent with our previous report (Inoue et al, 2010).

Figures 2(a) and 2(b) show the high pressure phase diagrams of wadsleyite and ringwoodite in the Mg_2SiO_4-Fe_2SiO_4 system under anhydrous and hydrous conditions, respectively, by using the present Fe/(Mg+Fe) data for wadsleyite and ringwoodite.

At 15.6 GPa (Run E1766), the coexistence of wadsleyite and ringwoodite starts to appear in the anhydrous system, but ringwoodite does not appear in the hydrous system. This trend for the anhydrous and hydrous systems continues up to 16.5 GPa (Run E1794), and the coexistence of wadsleyite and ringwoodite appears at 16.5 GPa (Run E1760, E1751) in the hydrous system. In run E1788 (P=~17 GPa), only ringwoodite was observed under anhydrous conditions, but the coexistence of wadsleyite and ringwoodite was still observed under hydrous conditions.

This result indicates that the loop of the wadsleyite and ringwoodite boundary shifts towards higher pressure or higher iron content, and the pressure width of the loop decreased with the effect of H_2O. The present observation is consistent with our previous result of 1 wt% H_2O (Inoue et al., 2010).

We have already determined that the phase boundary between olivine and wadsleyite shifts to lower pressures under water bearing conditions (Chen et al., 2002; Inoue et al., 2009). Combining the present results with our previous data, it is clear that the stability region of wadsleyite expands and the pressure width of the divariant loop decreases for both of the phase boundaries between olivine and wadsleyite, and between wadsleyite and ringwoodite.

In the present study, the experiments were performed under H_2O-rich fluid saturated conditions, so note that the width of the loop can only be applied to H_2O-rich fluid saturated conditions, and the width of the loop should be narrower than those in H_2O-rich fluid undersaturated conditions when considering the phase diagram of the pure-Mg system (Frost and Dolejs, 2007). However, the important point is that the amounts of Mg and Fe in the coexisting phases are different between anhydrous and hydrous conditions (Inoue et al.2010). The present results reflect the system with Mg-Fe partitioning under H_2O-rich fluid saturated condition.

For the hydrous melting phase relation, clinoenstatite was observed in the liquidus phase below ~17 GPa, and then changed to stishovite. These results indicate that MgO-rich (ultrabasic) liquid was formed under hydrous melting conditions, which are consistent with our previous results (Inoue at al., 1994; Yamada et al., 2004).

3-2. The effect of water on postspinel phase boundary

The coexisting region of ringwoodite and perovskite was quite narrow in both the anhydrous and hydrous systems, so it was difficult to determine the exact loop in this boundary. However, we could observe the coexistence of ringwoodite and perovskite at pressures of 23.0-23.2 GPa (runs E1784, E1730 and E1695).

At 23.0 GPa (E1784), the Fe/(Mg+Fe) ratios in ringwoodite, perovskite, and magnesiowustite were 0.199, 0.086 and 0.342, respectively, whereas in the hydrous system, the Fe/(Mg+Fe) ratios in ringwoodite and perovskite were 0.159 and 0.056, respectively. We could not observe magnesiowustite in the most hydrous run, because the composition of the hydrous liquid became MgO rich with increasing pressure, as we

have already reported (Inoue, 1994; Yamada et al., 2004), and magnesiowustite tends to dissolve in the liquid. The reason why the Fe/(Mg+Fe) ratios of ringwoodite and perovskite in the hydrous system is much lower than those in anhydrous conditions is the existence of the hydrous liquid. The hydrous liquid prefers iron compared to crystalline phases. Nevertheless, the partition coefficients, Kd = $(Fe/Mg)_{Pv}/(Fe/Mg)_{\gamma}$, were almost the same (~0.3~0.4) in both anhydrous and hydrous systems.

We have already reported the effect of water on the spinel-postspinel transformation in Mg_2SiO_4, and reported that the boundary moves to high pressures by ~0.2 GPa under water bearing conditions, compared with anhydrous conditions (Higo et al., 2001). In the present experiment, we could not observe the phenomena clearly because of the fluctuation of the generated pressure in each cell assembly. In the hydrous system this was also caused by the complicated phase assembly in each run. Nevertheless, the main purpose of the present experiment was to obtain the coexisting sample of ringwoodite and perovskite to determine the H_2O content and the partitioning effect. We succeeded in this purpose, which will be further described later.

3-3. The H_2O content and partitioning in wadsleyite, ringwoodite and prerovskite

We succeeded in synthesizing large (~50μm) crystals of coexisting wadsleyite and ringwoodite, and of ringwoodite and perovskite. Figures 3 and 4 show the back scattered electron images of the coexisting run products of wadsleyite and ringwoodite (E1751, E1760), and of ringwoodite and perovskite (E1748 and E1730), respectively. In all run products, hydrous liquids coexisted with the minerals. In addition, clinoenstatite existed in the liquidus phase at ~16.5 GPa and 1673K under hydrous melting conditions.

Table 6 shows the H_2O contents in wadsleyite and ringwoodite at ~16.5 GPa and 1673K, and the corresponding partition coefficient. The H_2O contents in wadsleyite and ringwoodite at ~16.5 GPa and 1673K were 1.8-2.3 wt% and 1-1.25 wt%, respectively. In E1788, the H_2O content was higher than that in the other runs, because the temperature was estimated by the power supply and the generated temperature may have been lower than 1673K. For this reason, the amount of hydrous melt was small and the H_2O contents in the crystals became higher in E1788. In spite of this difference, the partition coefficient between wadsleyite and ringwoodite ($Kd=(H_2O)_{\beta}/(H_2O)_{\gamma}$) was ~2;

this result shows that wadsleyite favors H_2O twice as much when compared to ringwoodite.

Table 7 shows the H_2O content in ringwoodite and perovskite at ~23 GPa and 1873K, and the partition coefficient. The H_2O content in ringwoodite and perovskite at ~23 GPa and 1873K were 0.6-0.8 wt% and less than 0.1 wt%, respectively. Because the H_2O content in perovskite was quite small, the resulting calculated partition coefficient between ringwoodite and perovskite exhibits larger scatter. Nevertheless, the results show that the partition coefficient between ringwoodite and perovskite ($Kd=(H_2O)_\gamma/(H_2O)_{Pv}$) could be determined to be ~15 in average; this result shows that ringwoodite favors H_2O 15 times more compared with perovskite.

We have already determined that the partition coefficient between olivine and wadsleyite ($Kd=(H_2O)_\beta/(H_2O)_\alpha$) was ~5 (Chen et al., 2002). Combining our previous data with our present data, the partitioning of H_2O in olivine(α), wadsleyite(β), ringwoodite(γ) and perovskite(Pv) could be determined as $\alpha : \beta : \gamma : Pv = 6 : 30 : 15 : 1$. Olivine is the most abundant minerals in the mantle, so the H_2O partitioning among the upper mantle, between 410-520 km and 520-660 km of the mantle transition zone, and the lower mantle can be estimated as 6:30:15:1, respectively.

Because the maximum H_2O solubility in wadsleyite is 3.3 wt% (e.g. Inoue et al, 1995), the possible maximum H_2O storage capacities in the olivine high pressure polymorphs are as follows; ~0.7 wt% in olivine (upper mantle just above 410 km depth), ~3.3 wt% in wadsleyite (410-520 km depth), ~1.7 wt% in ringwoodite (520-660 km depth) and ~0.1 wt% in perovskite (lower mantle). With this consideration, we adopted the maximum H_2O solubility in wadsleyite to discuss the maximum H_2O storage capacity in the mantle. However, it was reported that the H_2O solubility becomes lower with increasing temperature (e.g. Demouchy et al. 2005). The temperature in the mantle transition zone is important to estimate the H_2O content.

In spite of the effect of temperature, the mantle transition zone should be a large geochemical reservoir of water in the Earth's interior, and the maximum water storage capacity in the mantle transition zone is ~4 times relative to the amount of sea water. Note that the H_2O content in olivine was determined at ~13.5 GPa (just above 410 km depth), and we know that the H_2O solubility in olivine increases with increasing pressure as shown in Kohlstedt et al. (1996) and Hauri et al. (2006). In the shallower mantle below 410 km depth, the H_2O content in olivine should become less with

decreasing pressure.

3-4. Geophysical implication

Knowledge of absolute water contents in the mantle is important because hydration affects various physical properties of mantle minerals (e.g. Inoue et al, 1998; Jacobsen et al., 2004; Huang et al., 2005). Therefore, many researchers have made an effort to estimate the absolute water content in the mantle. Especially, seismological and electrical conductivity observations combined with laboratory measured values enable us to estimate the water content in the mantle. Mantle transition zone minerals, wadsleyite and ringwoodite, can accommodate significant amount of H_2O (up to 2-3 wt%) in their crystal structures, so these minerals should be key minerals to contain water in the mantle.

Suetsugu et al. (2006) and Yamada et al. (2009) tried to estimate temperature anomalies and water content in the mantle transition zone just above the 660 km discontinuity beneath the Japan Islands and the Philippine Sea from tomographically determined P-velocity anomalies and the depth of the 660-km discontinuity determined by the receiver function method. The water content beneath the Philippine Sea and western Japan, where the Pacific slab is subducted, was estimated to be in the range of 1-1.5 wt% H_2O, and the west Philippine basin, away from the Pacific slab, did not have any significant water content. This estimated H_2O content shows the relative water content anomaly with respect to average values in their study regions, because tomographically determined P-velocity anomalies were used as mentioned in Yamada et al. (2009). They observed the apparently unreasonable negative values of water content (-0.5 wt%) beneath northern Japan, and interpreted that the average H_2O content could be regarded as ~0.5 wt% in the region, when it is regarded as a situation of absolutely null water (dry). Recently, Suetsugu et al. (this issue) applied the same method by using a new data set of ocean bottom geophysical observations beneath the Philippine Sea and the northwestern Pacific Ocean, and revised the water content and estimated that there was less than 0.2 wt% H_2O beneath these areas. Although they mentioned that the estimated water content had an uncertainty of about 0.2-0.3 wt% H_2O, the average H_2O content in these areas was considered to be ~0.1 wt% H_2O from Figure 7 in Suetsugu et al. (this issue). Note that this estimated H_2O contents reflects that in ringwoodite.

296 On the other hand, the electrical conductivities of wadsleyite and ringwoodite in
297 anhydrous and hydrous forms were measured (Huang et al., 2005; Yoshino et al., 2008;
298 Manthilake et al., 2009; Dai and Karato, 2009), and compared to the geophysical
299 observations to estimate the water content. Though there are some arguments about the
300 estimated water content (Karato and Dai, 2009; Yoshino and Katsura, 2009), their recent
301 conclusions show that some water (~0.1–0.3 wt% in the Pacific) is required to explain
302 the observed electrical conductivity (Dai and Karato, 2009). In addition, though Yoshino
303 et al. (this issue) mentioned that the present conductivity-depth profiles in the transition
304 zone agreed with that obtained from the geophysical observations beneath the Pacific in
305 the case of the mantle transition zone, 0.1-0.2 wt% H_2O explains the recent geophysical
306 reference model (Shimizu et al., submitted) from Figure 6 in Yoshino et al. (this issue).
307 Still more, Yoshino et al. (this issue) mentioned that the presence of water in the
308 transition zone minerals is required to explain the high conductivity beneath the
309 Philippine Sea and northeastern China (Baba et al., this issue).
310 In this study, we determined the partitioning of H_2O among olivine high pressure
311 polymorphs. When we apply ~0.2 wt% of the H_2O content in wadsleyite in the mantle
312 transition zone estimated by the recent electrical conductivity measurements (e.g. Dai
313 and Karato, 2009), the estimated H_2O content in the mantle is as follows; ~0.04 wt% in
314 olivine (upper mantle), ~0.2 wt% in wadsleyite (410-520 km depth), ~0.1 wt% in
315 ringwoodite (520-660 km depth), and ~0.007 wt% in perovskite (lower mantle). These
316 estimated values satisfy, within the error, the recently estimated H_2O content in mantle
317 transition zone minerals (i.e. wadsleyite and ringwoodite) by different methods based on
318 seismological and electrical conductivity observations.
319 Thus, the mantle transition zone should be a large geochemical reservoir of water in
320 the Earth's mantle compared with the upper and lower mantle. Additionally, the amount
321 of water in the mantle transition zone is ~0.3 times more relative to that of sea water,
322 when mantle wadsleyite contains ~0.2 wt% H_2O.
323
324 **4. Conclusions**
325 We have determined the water partitioning between wadsleyite and ringwoodite, and
326 ringwoodite and perovskite. The results are as follows; olivine : wadsleyite :
327 ringwoodite : perovskite = 6: 30: 15 : 1. In addition, the phase boundary of
328 olivine-wadsleyite, wadsleyite-ringwoodite, and postspinel transformations move to the

low, high, and high pressure side, respectively, with the effect of water, when we combine the present data with our previous data (Higo et al., 2001; Chen et al., 2002; Inoue et al., 2010). The resultant H_2O partitioning of $[H_2O]_\alpha < [H_2O]_\beta > [H_2O]_\gamma > [H_2O]_{pv}$ is consistent with the results of the effect of water on the high pressure phase boundary of olivine.

Because the maximum H_2O solubility in wadsleyite is 3.3 wt% (e.g. Inoue et al, 1995), the possible maximum H_2O storage capacity in the olivine high pressure polymorphs are as follows; ~0.7 wt% in olivine (upper mantle just above 410 km depth), ~3.3 wt% in wadsleyite (410-520 km depth), ~1.7 wt% in ringwoodite (520-660 km depth), and ~0.1 wt% in perovskite (lower mantle).

When we apply ~0.2 wt% of the H_2O content in wadsleyite in the mantle transition zone, the estimated H_2O content through the mantle are as follows; ~0.04 wt% in olivine (upper mantle just above 410 km depth), ~0.2 wt% in wadsleyite (410-520 km depth), ~0.1 wt% in ringwoodite (520-660 km depth), and ~0.007 wt% in perovskite (lower mantle).

Thus, the mantle transition zone should contain a large water reservoir in the Earth's mantle when compared to the upper and lower mantle. Additionally, if mantle wadsleyite contains ~0.2 wt% H_2O then the mantle transition zone would contain approximately one-third the H_2O mass of Earth's oceans.

Acknowledgements

We thank the constructive comments of two reviewers Dr. M. Akaogi and Dr. S.D. Jacobsen to improve the manuscript. We also thank Sabrina Whitaker at the GRC, Ehime University for the English improvement. This work was supported by a Grant-in-Aid for Scientific Research (A) [KAKENHI] from Japan Society for the Promotion of Science (JSPS) given to Toru Inoue, and a Global COE program from the Ministry of Education, Culture, Sports, Science and Technology (MEXT).

References

Akaogi, M., Ito, E., Novrotsky. A., 1989. Olivine-modified spinel-spinel transitions in the system Mg_2SiO_4-Fe_2SiO_4: Calorimetric measurements, thermochemical calculation, and geophysical application, J. Geophys. Res., 94, 15671-15685.

Baba, K., Utada, H., Goto, T., Kasaya, T., Shimizu, H., Tada, N., Electrical conductivity imaging of the Philippine Sea upper mantle using seafloor magnetotelluric data. Phys. Earth Planet. Inter. (this issue)

Bolfan-Casanova, N., H. Keppler, Rubie, D.C., 2003. Water partitioning at 660 km depth and evidence for very low water solubility in magnesium silicate perovskite, Geophys. Res. Lett., 30, 1905, doi: 10.1029/2003GL017182.

Brown, J.M. and Shankland, T.J., 1981. Thermodynamic parameters in the Earth as determined from seismic profiles. Geophys. J., Royal Astronomical Society, 66(3), 579-596.

Chen, J., Inoue, T., Yurimoto, H., Weidner, D.J., 2002. Effect of water on olivine-wadsleyite phase bondary in the $(Mg, Fe)_2SiO_4$ system, Geophys. Res. Lett., 29, 1875, doi:10.1029/2001GL014429.

Dai, L., Karato, S. 2009. Electrical conductivity of wadsleyite at high temperatures and high pressures. Earth Planet. Sci. Lett., in press.

Demouchy, S., Deloule, D., Frost, D.J., Keppler, H., 2005. Pressure and temperature dependence of water solubility in Fe-free wadsleyite. Am. Mineral., 90, 1084-1091.

Frost, D. J., Dolejs, D, 2007. Experimental derteimination of the effect of H_2O on the 410-km seismic discontinuity. Earth Planet. Sci. Lett., 256, 182-195.

Hauri, E.H., Gaetani, G.A., Green, T.H., 2006. Partitioning of water during melting of the Earth's upper mantle at H2O-undersaturated conditions. Earth Planet. Sci. Lett., 248, 715-734.

Higo, Y., Inoue, T., Irifune T., Yurimoto, H., 2001. Effect of water on the spinel-postspinel transformation in Mg_2SiO_4. Geophys. Res. Lett., 28, 3505-3508.

Huang, X., Xu, Y., Karato, S., 2005. Water content in the transition zone from electrical conductivity of wadsleyite and ringwoodite. Nature, 434, 746-749.

Inoue, T., 1994. Effect of water on melting phase relations and melt composition in the system Mg_2SiO_4-$MgSiO_3$-H_2O up to 15 GPa. Phys. Earth Planet. Inter., 85, 237-263.

Inoue, T., Yurimoto H., Kudoh, Y., 1995. Hydrous modified spinel, $Mg_{1.75}SiH_{0.5}O_4$: a new water reservoir in the mantle transition region, Geophys. Res. Lett., 22, 117-120.

393 Inoue, T., Weidner, D.J., Northrup P.A., Parise, J.B., 1998. Elastic properties of hydrous
394 ringwoodite (γ-phase) on Mg_2SiO_4, Earth Planet. Sci. Lett., 160, 107-113.
395 Inoue, T. Ueda, T., Tanimoto, Y., Yamada, A., Irifune, T., 2010. The effect of water on
396 the high-pressure phase boundaries in the system Mg_2SiO_4-Fe_2SiO_4. J. Phys.: Conf.
397 Ser., 215, 012101.
398 Jacobsen, S.D., Smyth, J.R., Spetzler, H., Holl, C.M., Frost, D.J., 2004. Sound
399 velocities and elastic constants of iron-bearing hydrous ringwoodite. Phys. Earth
400 Planet. Inter., 143-144, 47-56.
401 Irifune, T., Kubo, N., Isshiki, M., Yamazaki, Y., 1998. Phase transformations in
402 serpentine and transportation of water into the lower mantle. Geophys. Res. Lett.,
403 25, 203-206.
404 Ito, E., Takahashi, E., 1989. Postspinel transformations in the system Mg_2SiO_4-Fe_2SiO_4
405 and some geophysical implications, J. Geophys. Res., 94, 10,637-10,646.
406 Karato, S., Dai, L., 2009. Comments on "Electrical conductivity of wadsleyite as a
407 function of temperature and water content" by Manthilake et al., Phys. Earth Planet.
408 Inter., 174, 19-21.
409 Katsura, T., Shatskiy, A., Manthilake, M.A.G.M., Zhai, S., Fukui, H., Yamazaki, D.,
410 Matsuzaki, T., Yoneda, A., Ito, E., Kuwata, A., Ueda, A., Nozawa, A., Funakoshi,
411 K., 2009. Thermal expansion of forsterite at high pressures determined by in situ
412 X-ray diffraction: The adiabatic geotherm in the upper mantle. Phys. Earth Planet.
413 Inter., 174, 86-92.
414 Kohlstedt, D.L., Keppler, H., Rubie, D.C., 1996. Solubility of water in the α, β and γ
415 phases of $(Mg,Fe)_2SiO_4$. Contrib. Mineral. Petrol., 123, 345-357.
416 Kurosawa, M., Yurimoto, H., Sueno, S., 1997. Patterns in the hydrogen and trace
417 element compositions of mantle olivines. Phys. Chem. Minerals, 24, 385-395.
418 Manthilake, M.A.G.M., Matsuzaki, T., Yoshino, T., Yamashita, S., Ito, E., Kastura, T.,
419 2009. Electrical conductivity of wadsleyite as a function of temperature and water
420 content. Phys. Earth Planet. Inter., 174, 10-18.
421 Mibe, K. Kanzaki, M., Kawamoto, T., Matsukage, K.N., Fei, Y., Ono, S., 2007. Second
422 critical end point in the peridotite-H2O system. J. Geophys. Res., 112, B03201.
423 Miyagi, I., Yurimoto, H., 1995. Water content of melt inclusions in phenocrysts using
424 secondary ion mass spectrometer. Bull. Volcanol. Soc. Jpn., 40, 349-355.

425 Miyagi, I. Matsubaya, O., Nakashima, S., 1998. Change in D/H ratio, water content and
426 color during dehaydration of hornblende. Geochem. J., 32, 33-48.
427 Ohtani, E., Litasov, K., Hosoya, T., Kubo, T., Kondo, T., 2004. Water transport into
428 deep mantle and formation of a hydrous transition zone, Phys. Earth Planet. Inter.,
429 143-144, 255-269.
430 Shimizu, H. Koyama, T., Baba, H., Utada, H. Revised 1-D mantle electrical
431 conductivity structure beneath the north Pacific. Geophys. Int. J. (submitted)
432 Suetsugu, D., Inoue, T. Yamada, A., Zhao, D., Obayashi, M., 2006. Towards mapping
433 the three-dimentinal distribution of water in the transition zone from P-velocity
434 tomography and 660-km discontinuity depths. In "Earth's deep water cycle,
435 Geophysical monograph series 168", Ed. by Steven D. Jacobsen and Suzan van
436 der Lee, AGU, pp.237-249.
437 Suetsugu, D., Inoue, T., Obayashi, M., Yamada, A., Shiobara, H., Sugioka, H., Ito, A.,
438 Kanazawa, T., Kawakatsu, H., Shito, A., Fukao, Y. Depths of the 410-km and
439 660-km discontinuities in and around the stagnant slab beneath the Philippine Sea:
440 Is water stored in the stagnant slab? Phys. Earth Planet. Inter. (this issue)
441 Yamada, A., Inoue, T., Irifune, T., 2004. Melting of enstatite from 13 to 18 GPa under
442 hydrous conditions, Phys. Earth Planet. Inter., 147, 45-56.
443 Yamada, A., Zhao, D., Inoue, T., Suetsugu, D., Obayashi, M., 2009. Seismological
444 evidence for compositional variations at the base of the mantle transition zone
445 under Japan Islands, Gondwana Research , 16, 482-490.
446 Yoshino, T., Manthilake, G., ,Matsuzaki, T., Katsura, T., 2008. Dry mantle transition
447 zone inferred from electrical conductivity of wadsleyite and rinwwoodite. Nature
448 451, 326-329.
449 Yoshino, T., Katsura, T., 2009. Reply to Comments on “Electrical conductivity of
450 wadsleyite as a function of temperature and water content” by Manthilake et al.,
451 Phys. Earth Planet. Inter., 174, 22-23.
452 Yoshino, T., Katsura, T., Baba, K., Utada, H. Laboratory-based conductivity structure in
453 the mantle transition zone. Phys. Earth Planet. Inter. (this issue)
454 Yurimoto, H., Kurosawa, M., Sueno, S. 1989. Hydrogen analysis in quartz crystals and
455 quartz glass by secondary ion mass spectrometry. Geochim. Cosmochim. Acta 53,
456 751-755.

Figure captions

Figure 1. An example of the cell assembly used in the present experiments for the wadsleyite-ringwoodite transformation.

Figure 2. (a) High pressure phase diagram of olivine high pressure polymorphs under anhydrous condition at T=1673K. The solid line represents the phase boundary from Akaogi et al. (1989) under anhydrous condition. Using this plot, the run pressures were determined.
(b) High pressure phase diagram of olivine high pressure polymorphs under hydrous condition at T=1673K. The broken line represents the phase boundary from Akaogi et al. (1989) under anhydrous condition, and the solid line represents that under hydrous condition from Inoue et al. (2010). The present results are consistent with our previous boundary of Inoue et al. (2010).
Open triangles and squares show the assemblages of the single wadsleyite phase and that of the single ringwoodite phase, respectively, and filled triangles and squares show the wadsleyite coexisting with ringwoodite, and the ringwoodite coexisting with wadsleyite, respectively. α: olivine, β: wadsleyite, γ: ringwoodite.

Figure 3. Back scattered electron image of run products (a) E1751 and (b) E1760. β: wadsleyite, γ: ringwoodite, CEn: clinoenstatite, L: liquid.

Figure 4. Back scattered electron image of run products (a) E1784 and (b) E1730. γ: ringwoodite, Pv: perovskite, L: liquid.

Fig1

Click here to download Figure(s): Fig1.pptx

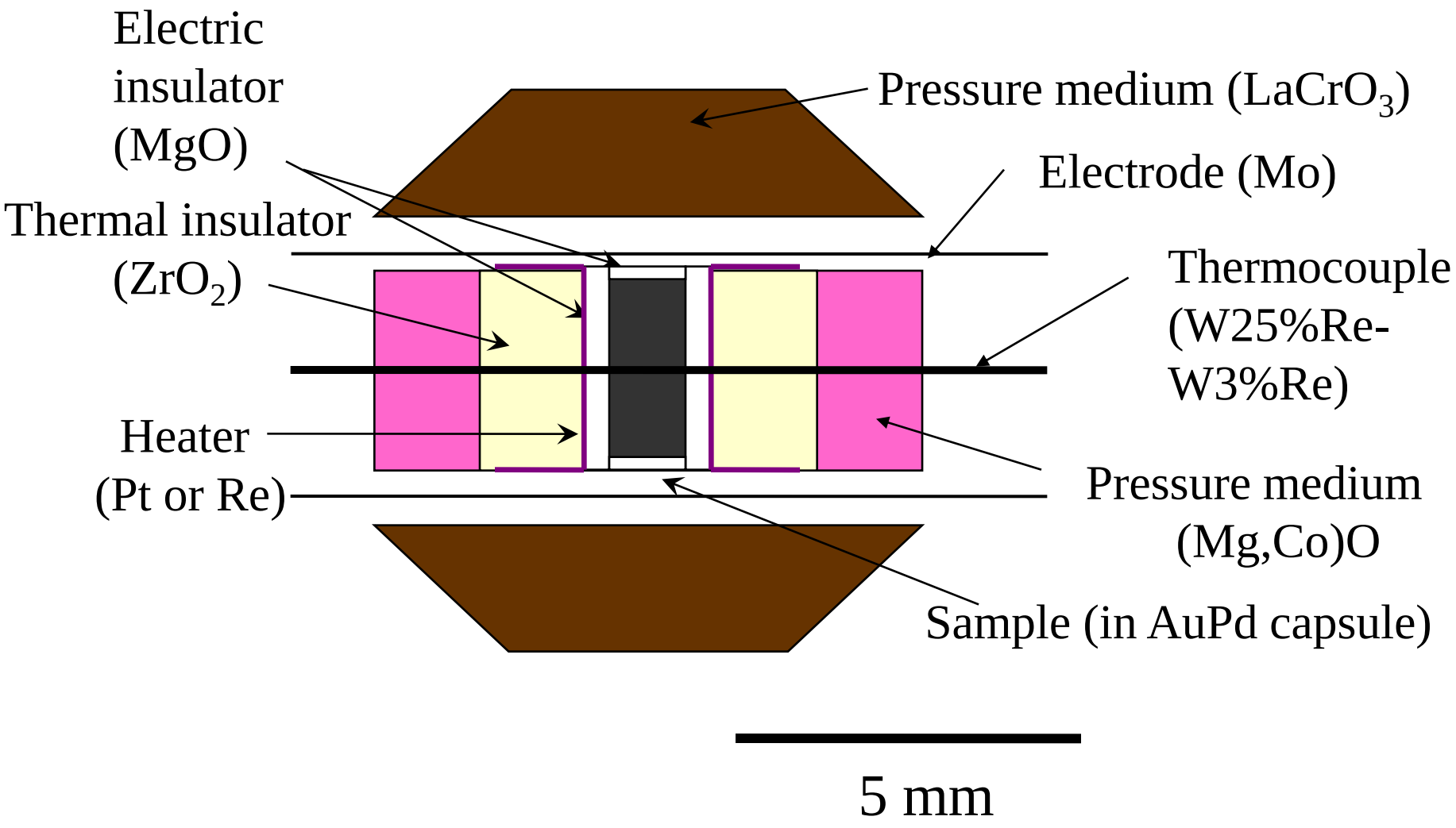

Fig. 1 Inoue et al.

Fig2a
Click here to download Figure(s): Fig2a.ppt

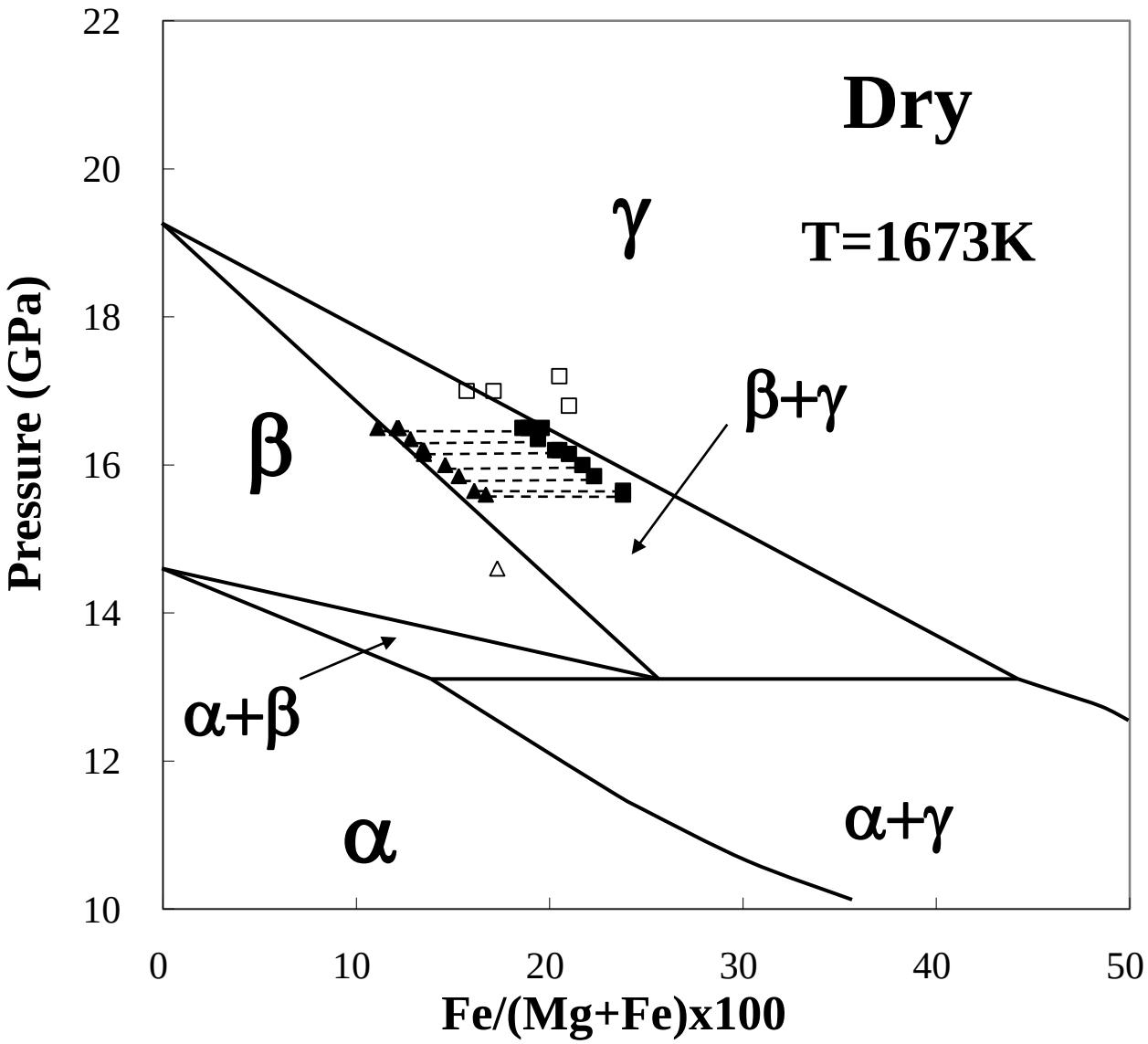

Fig. 2 (a) Inoue et al.

Fig2b
Click here to download Figure(s): Fig2b_revised.ppt

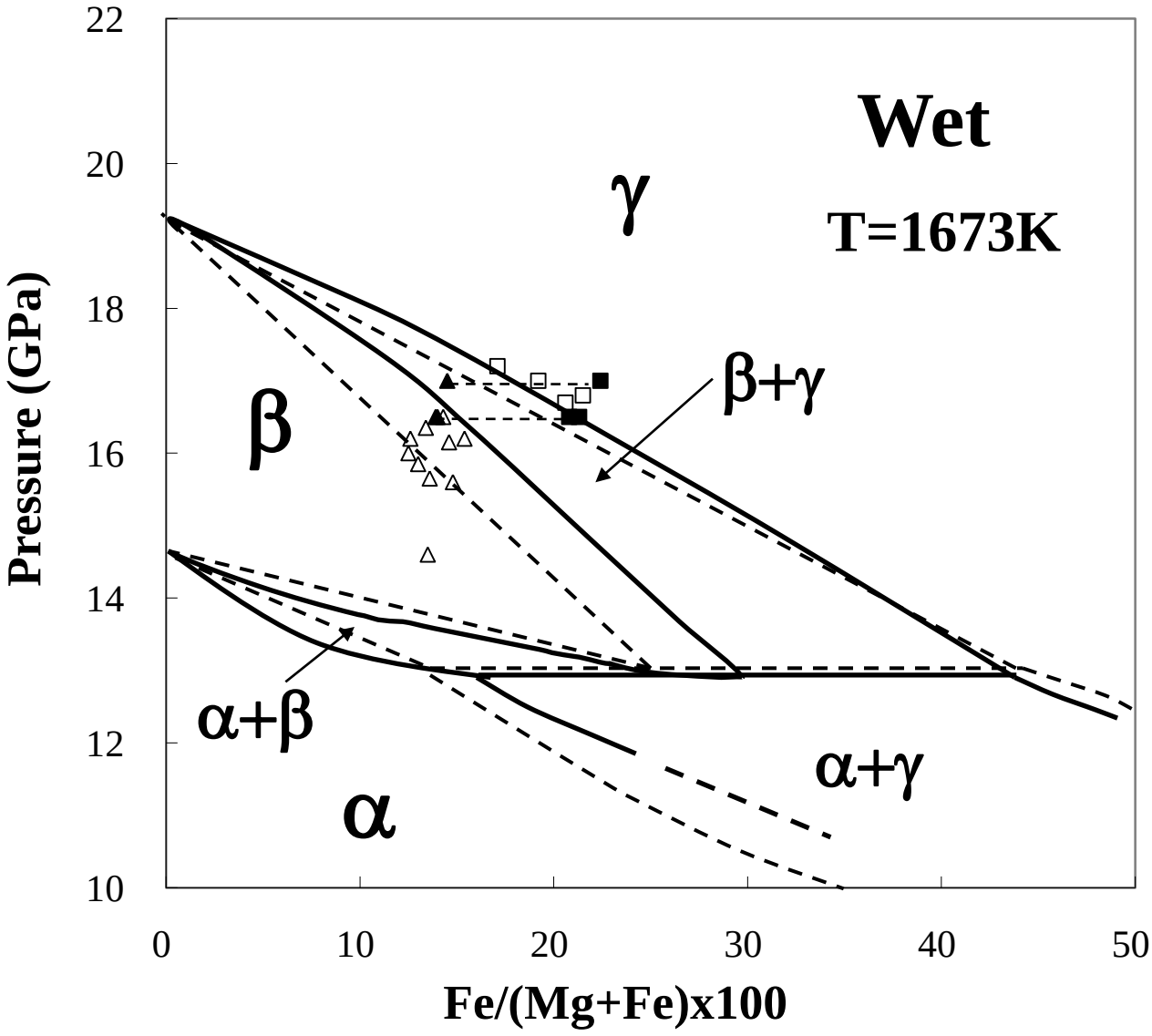

Fig. 2 (b) Inoue et al.

Fig3
Click here to download Figure(s): Fig3.ppt

(a) E1751 WET
16.5GPa, 1673K

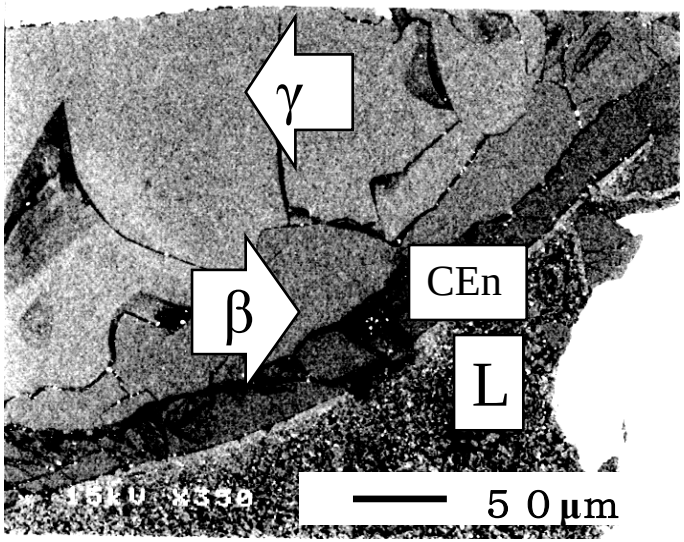

(b) E1760 WET
16.5GPa, 1673K

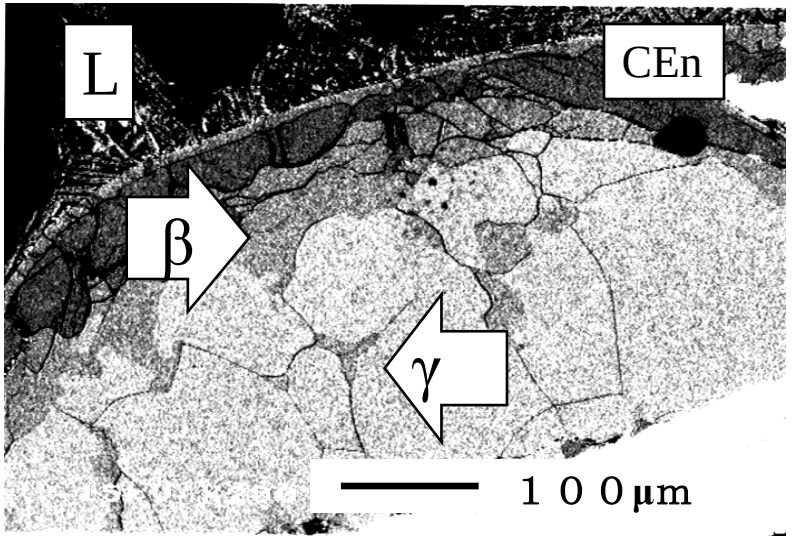

Fig. 3 Inoue et al.

Fig4
Click here to download Figure(s): Fig4.ppt

(a) E1784 WET
23.0GPa, 1873K

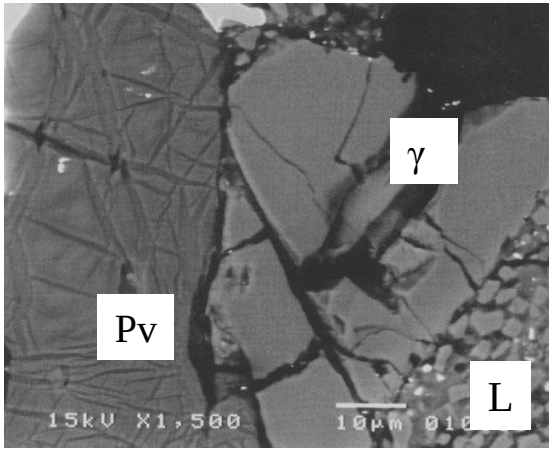

(b) E1730 WET
23.1GPa, 1873K

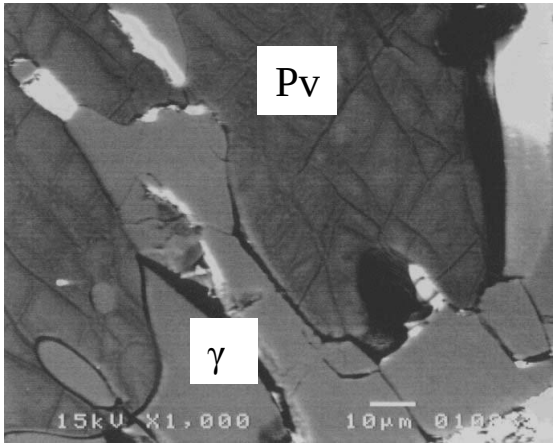

Fig. 4 Inoue et al.

Table1

Table 1. Chemical composition of starting material

	Dry	Wet
MgO	42.1	35.4
FeO	18.7	15.8
SiO_2	39.2	33.0
H_2O	-	15.8
Total (wt%)	100.0	100.0
(Mg+Fe)/Si	2.0	2.0
Fe/(Mg+Fe)	0.2	0.2

Dry: $Fe_2SiO_4+8MgO+4SiO_2 \rightarrow 5(Mg_{0.8}Fe_{0.2})_2SiO_4$

Wet: $Fe_2SiO_4+8Mg(OH)_2+4SiO_2 \rightarrow 5(Mg_{0.8}Fe_{0.2})_2SiO_4+H_2O$

Table2

Table 2. Experimental conditions and the results (T=1673K)

Run No.	Load (ton)	Pressure (GPa)	Time (min)	Dry	Wet
E1672	412	14.6	60	β	β＋L
E1766	480	15.6	120	β＋γ	β＋CEn＋L
E1748	470	15.7	60	β＋γ	β＋CEn＋L
E1678	500	15.9	60	β＋γ	β＋CEn＋L
E1789	490	16.0	60	β＋γ	β＋L
E1786	483	16.2	90	β＋γ	β＋CEn＋L
E1805	506	16.2	90	β＋γ	β＋CEn＋L
E1744	505	16.2	60	β＋γ	β＋CEn＋L
E1807	506	16.4	90	β＋γ	β＋CEn＋L
E1794	500	16.5	90	β＋γ	β＋L
E1760	485	16.5	90	β＋γ	β＋γ＋CEn＋L
E1751	510	16.5	120	β＋γ	β＋γ＋CEn＋L
E1788*	485	~17#	60	γ	β＋γ+CEn＋L
E1758	508	~17#	60	γ	γ＋St＋L
E1738*	520	16.7	60	γ	γ＋L
E1731	525	16.8	60	γ	γ＋L
E1683	550	17.2	60	γ	γ＋L

β: wadsleyite, γ: ringwoodite, CEn: clinoenstatite, St: stishovite, L: liquid

* Temperatures were estimated by power supply.

These pressure should have large uncertainty.

Table3

Table 3. Experimental conditions and the results (T=1873K)

Run No.	Load (ton)	Pressure (GPa)	Time (min)	Dry	Wet
E1720	435	22.9	60	γ	Pv + L
E1767	435	22.9	120	γ#	SuB+D+Mw+L
E1749*	440	23.0	120	γ#	Pv + L
E1759*	440	23.0	120	γ#	Pv+Mw+SuB+L
E1770	440	23.0	120	Pv + Mw	Pv + Mw + L
E1784*	440	23.0	20	γ + Pv +Mw	γ + Pv + L
E1730	445	23.1	60	γ + Pv + Mw	γ + Pv + L
E1787	445	23.1	60	γ	Pv + L
E1688	450	23.2	60	γ + Pv + Mw	Pv + L
E1695	450	23.2	30	γ + Pv + Mw	γ + Pv + L
E1796	450	23.2	60	γ#	γ+Mw+SuB+D+L

γ：ringwoodite, Pv：perovskite, Mw：magnesiowustite, St：stishovite
SuB：superhydrous phase B, D：phase D, L：liquid
*Temperatures were estimated by power supply.
#Small amounts of magnesiowustite and stishovite exist in the run charge.

Table4

Table 4. Fe/(Mg+Fe) in β and γ and the partitioning (T=1673K)

Run No.	Pressure	Dry			Wet		
		Fe/(Mg+Fe)			Fe/(Mg+Fe)		
	(GPa)	β	γ	Kd	β	γ	Kd
E1672	14.6	0.173(6)	----		0.135(5)	----	
E1766	15.6	0.167(1)	0.238(4)	1.56	0.148(28)	----	
E1748	15.7	0.161(4)	0.238(11)	1.62	0.136(3)	----	
E1678	15.9	0.153(1)	0.223(2)	1.59	0.130(4)	----	
E1789	16.0	0.146(2)	0.217(2)	1.62	0.125(1)	----	
E1786	16.2	0.135(7)	0.210(6)	1.71	0.146(3)	----	
E1805	16.2	0.134(6)	0.205(5)	1.67	0.154(7)	----	
E1744	16.2	0.135(1)	0.203(6)	1.64	0.126(5)	----	
E1807	16.4	0.128(3)	0.194(2)	1.65	0.134(2)	----	
E1794	16.5	0.122(1)	0.186(5)	1.65	0.143(11)	----	
E1760	16.5	0.121(5)	0.189(6)	1.70	0.139(4)	0.213(8)	1.68
E1751	16.5	0.111(4)	0.196(3)	1.95	0.140(5)	0.208(3)	1.62
E1788*	~17#	----	0.157(6)		0.145(3)	0.224(3)	1.70
E1758	~17#	----	0.171(5)		----	0.192(6)	
E1738*	16.7		N.A.		----	0.206(4)	
E1731	16.8	----	0.210(2)		----	0.215(2)	
E1683	17.2	----	0.205(2)		----	0.171(14)	

( ): standard deviation; N.A. not analyzed; * Temperatures were estimated by power supply.

Kd = $(Fe/Mg)_{\gamma}$ / $(Fe/Mg)_{\beta}$; # These pressure should have large uncertainty.

Table5

Table 5. Fe/(Mg+Fe) in γ and perovskite and the partitioning (T=1873K)

Run No.	Pressure	Dry				Wet	
		Fe/(Mg+Fe)				Fe/(Mg+Fe)	
	(GPa)	γ	Pv	Mw	Kd	γ	Pv
E1784*	23.0	0.199(9)	0.086(1)	0.342(2)	0.38	0.159(1)	0.056(3)
E1730	23.1	0.188(1)	N.A.	N.A.		0.135(2)	0.063(4)
E1695	23.2	0.178(4)	0.084(6)	N.A.	0.42	0.087(2)	0.049(3)

( ): standard deviation; N.A. not analyzed; * Temperatures were estimated by power supply.
$Kd = (Fe/Mg)_{Pv} / (Fe/Mg)_{\gamma}$

Table6

Table 6. H_2O partitioning between wadsleyite (β) and ringwoodite (γ)
T=1673K

Run No.	Pressure (GPa)	H_2O wt%		Kd
		β	γ	
E1788*-1	~17	3.72	1.69	2.2
E1760-1	16.5	2.28	1.11	2.05
E1760-2	16.5	2.24	1.25	1.79
E1751-1	16.5	1.88	1	1.88
E1751-2	16.5	1.79	1.1	1.63
average				1.9(2)

* Temperature was estimated by power supply.

( ): standard deviation, $Kd=(H_2O)_\beta/(H_2O)_\gamma$

Table7

Table 7. H_2O partitioning between ringwoodite (γ) and perovskite (Pv)
T=1873K

Run No.	Pressure	H_2O wt%		Kd
	(GPa)	γ	Pv	
E1784*	23	0.76	0.06	13
E1730	23.1	0.71(25)	0.03	24(8)
E1695	23.2	0.63(11)	0.07(3)	9(5)
average				15(8)

* Temperature was estimated by power supply.

( ): standard deviation, $Kd=(H_2O)_{\gamma}/(H_2O)_{Pv}$